THE PUBLISHING HOUSE
OF THE ROMANIAN ACADEMY

PROCEEDINGS OF THE ROMANIAN ACADEMY, Series A,
Volume 26, Number 1/2025, pp. 53–61
DOI: 10.59277/PRA-SER.A.26.1.08

OVERCOMING EFFICIENCY BOTTLENECKS IN ZRS_2 / GO PEROVSKITE SOLAR CELLS: A THEORETICAL EXPLORATION OF $MAPBI_3$ INTERLAYER IMPACT USING SCAPS-1D SIMULATION

Hmoud AL DMOUR[1], Saleh R. AL-BASHAISH[2], Osama Y. AL-MADANAT[3], Ahmad M.D. (Assa'd) JABER[4], Beddiaf ZAIDI[5], Marwan S. MOUSA[6], Emad K. JARADAT[7], Ahmad HAKAMY[8], Na'il SALEH[9], Fethi KOOLI[10]

[1] Mu'tah University, Faculty of Science, Department of Physics, Mu'tah 6170, Jordan, E-mail: hmoud79@mutah.edu.jo
[2] Al-Ahliyya Amman University, Faculty of Arts and Sciences, Department of Allied Sciences, Amman 19328, Jordan
[3] Mu'tah University, Faculty of Science, Department of Chemistry, Mu'tah 6170, Jordan
[4] Aqaba Medical Sciences University, Department of Basic Medical Sciences, Aqaba 77110, Jordan
E-mail: ahmad.jabr@amsu.edu.jo
[5] University of Batna 1, Faculty of Material Sciences, Algeria, Department of Physics, E-mail: beddiaf.zaidi@univ-batna.dz
[6] Jadara University, Department of Renewable Energy Engineering, Irbid 21110, Jordan, E-mail: marwansmousa@yahoo.com
[7] Imam Mohammad Ibn Saud Islamic University (IMSIU), Faculty of Science, Department of Physics, Riyadh 11623, Saudi Arabia
E-mail: ekyjaradat@imamu.edu.sa
[8] Umm Al-qura University, Faculty of Applied Science, Department of Physics, Makkah, 21955, Saudi Arabia
[9] United Arab Emirates University, College of Science, Department of Chemistry, P.o. Box 15551, Al Ain, United Arab Emirates
[10] Islamic University of Madinah, Faculty of Science, Department of Chemistry, Madinah 42351, Saudi Arabia,
E-mail: fethi_kooli@yahoo.com
Corresponding author: Hmoud AL DMOUR, E-mail: hmoud79@mutah.edu.jo

Abstract. One of the important factors in organic/inorganic solar cells is to have a large open circuit voltage for obtaining high power conversion efficiency. To achieve this aim, the effect of Methylammonium Lead Iodide ($MAPbI_3$) on the parameters of zirconium disulfide (ZrS_2) /graphene oxide (GO) hetero-junction solar cells was examined theoretically using a Solar Cell Capacitance Simulator (SCAPS-1D). The insertion of the $MAPbI_3$ layer between ZrS_2 and GO layers in the solar cell has resulted in notable improvements in the open circuit voltage, V_{oc}, from 0.55 V to 0.9 V, the power conversion efficiency, η, from 17% to 26% and short circuit current, J_{sc}, from 38.2 mA/cm^2 to 38.3 mA/cm^2, compared to the ZrS_2/GO solar cells. These data indicate that GO/$MAPbI_3$/ZrS_2 solar cells exhibit longer carrier lifetimes due to the multiple junctions and band-gap variations between GO/$MAPbI_3$ and $MAPbI_3$/ZrS_2 layers. Meanwhile, GO/ZrS_2 solar cells lack these additional junctions and band-gap variations, leading to lower efficiency and open-circuit voltage due to less effective light absorption and increased carrier recombination with faster carrier dynamics. Additionally, the onset voltage of capacitance of GO/$MAPbI_3$/ZrS_2 solar cell was higher than GO/ZrS_2 solar cell due to the energy levels of $MAPbI_3$ layer that formed between ZrS_2 and GO leading to an improvement in the open circuit voltage by around 80%. This latter finding has been confirmed by comparing the capacitance-frequency characteristics of the two solar cells. This work provides new insights into the synergistic effects of these materials, demonstrating how bandgap engineering and multiple junctions can significantly enhance solar cell performance.

Keywords*:* solar cells, open circuit voltage, multiple junctions, SCAPS-1D simulation.

1. INTRODUCTION

In recent decades, extensive research has focused on finding alternatives to fossil fuels in industrial development [1, 2], which is driven by environmental issues associated with fossil fuel use, including greenhouse gas emissions, air pollution, and human contributions to climate change [2–4]. Solar energy emerges as one of the most promising alternatives since it is friendly to the environment and available worldwide [5, 6]. Hence, it can be harvested through the use of solar cells to convert energy from sunlight to electricity and concentrated solar power [7–11].

The technology of solar cells has been extensively studied based on designs, materials used, and time frames. Solar cells are categorized into four generations based on their effectiveness and durability over time.

The initial generation featured thin-film cells made from silicon single-crystal or polycrystalline silicon. While various materials like amorphous silicon (a-Si), copper indium gallium selenide (CIGS), and cadmium telluride (CdTe) were employed in the next generation. To improve efficiency, new technology and materials such as organic solar cells, quantum dot solar cells, and dye-sensitized solar cells (DSSCs) have started to come into use in a bid to increase efficiency and counteract environmental concerns [12−15]. In the development of the first three generations, a lot of work has yet to be done in terms of efficiency, long life, and expensive production costs [16, 17].

Currently, the fourth generation of solar cells, perovskite solar cells (PSCs), have generated significant attention owing to their excellent power conversion efficiency (PCE) and the potential to overcome many of the shortfalls for previous generations of solar cell technologies [18, 19]. Perovskite solar cells started to get some attention after Tsutomu Miyasaka and coworkers made a publication in 2009 showing that 3.8% power conversion would be possible with a perovskite solar cell with mesoporous TiO_2 scaffold [18, 20]. Since then, the PCE of PSCs has stepped forward to attain over 25%, leading to providing an alternative solar cell technology to the Si, CdTe, and copper indium gallium commercial solar cells [13, 21].

Methylammonium lead iodide ($MAPbI_3$) is one of the wide spectrums of perovskite materials that have been experimented with and used to fabricate high-efficiency solar cells. It is a type of organic-inorganic hybrid perovskite material consisting of lead (Pb) as the central cation, iodine (I) as the anion, and methylammonium as the organic component [22, 23]. This specific combination of elements forms a semiconductor material with excellent light-absorbing properties. According to the National Renewable Energy Laboratory, MAPbI3 Perovskite solar cells have exhibited impressive PCEs exceeding 25% [21], which is higher than some of the best commercial silicon-based solar cells.

In the last decade, zirconium disulfide (ZrS_2) and Graphene oxide (GO) have received significant attention because they act as electron and hole transport materials, respectively, in perovskite solar cells [10, 11, 15, 24]. GO material characteristics with excellent transparency, low production cost, good solubility in many solvents, and high hole mobility, make it preferable in synthesizing solar cells. In 2022, Jeong *et al*. studied the effect of the GO and reduced GO intermediate layers on the efficiency of CZTSSe solar cells [25]. On the other hand, ZrS_2 material has high electron mobility and small suitable band alignment, make it a viable candidate for improving the efficiency of perovskite solar cells. It can be synthesized as a thin film for application in solar cell technologies. For instance, it was shown that ZrS_2 can be utilized as a buffer layer in CIGS solar cells [15]. Recent studies have demonstrated that ZrS_2 can be effectively utilized in a heterojunction configuration with $MAPbI_3$, leading to enhanced charge transport and reduced recombination losses [24]. Abdelfatah *et al*., in their simulations, indicate that solar cells employing ZrS_2 as the ETL can achieve comparable efficiencies to those using traditional materials such as In_2S_3, with reported efficiencies ranging from 16.94% to 22.50% [23]. This is particularly significant as the efficiency of PSCs has been a critical factor in their commercial viability, with $MAPbI_3$-based devices already reaching efficiencies above 20% [26, 27].

In this context, it has been found that the effect of the $MAPbI_3$ layer on the performance of ZrS_2/GO solar cells has not been studied in the literature. However, these materials exhibit promising electronic and optical properties, which align with the goal of enhancing solar cell efficiency. The combination of ZrS_2, GO, and $MAPbI_3$ into a single heterojunction could offer new insights into the synergistic effects of these materials. Therefore, in this study, the SCAPS-1D simulation is proposed to study the current density characteristics and the capacitance response of heterojunction solar cells composed of ZrS_2 / GO two layers and ZrS_2/ $MAPbI_3$/ GO three layers. The results here indicate that the $MAPbI_3$ layer modifies the interface characteristics between the GO and ZrS_2 layers, resulting in enhanced efficiency of the GO/ZrS_2 solar cell, addressing key challenges such as carrier recombination and light absorption.

2. DEVICE SIMULATION

By far, it was believed that numerical simulation can play a crucial role in understanding the performance optimization of different structures of solar cells. It has been used for several purposes; firstly, to model the physical processes occurring within solar cells and secondly, to predict the performance of solar cells under various conditions, such as different levels of sunlight intensity, temperature, and angles of incidence. SCAPS-1D is a specialized simulation tool that was mainly developed to simulate and assess the performance of

semiconductor-based solar cells properties, specifically focusing on their electrical characteristics in illuminated (light) and non-illuminated (dark) conditions [28]. Indeed, it was initially utilized for simulating the behavior of solar cells composed of $CuInSe_2$ and the CdTe family of materials [29]. The SCAPS-1D working principle is based on solving the essential semiconductor equations, *i.e.*, the Poisson equation (1), the continuity equations for electrons and holes (2 and 3), and the drift-diffusion equations of the hole and electron carrier transport properties (4 and 5) [30]. These equations are essential to understand the behavior and performance of solar cells.

$$\frac{\dot{\mathrm{d}}^2\,\phi}{\mathrm{d}x^2} + \frac{q}{\varepsilon}\left[\,p(x) - n(x) + N_D - N_A + \,\rho_{\,p} - \,\rho_{\,n}\right] = 0 \tag{1}$$

where ψ is electrostatic potential, ε is dielectric constant, q is electron charge, p is free hole density, n is free electron density, N_D represents ionized acceptors, N_A is donor density, and ρ_p and ρ_n are the hole and electron distributions, respectively.

$$\frac{1}{q}\frac{\dot{\mathrm{d}}J_P}{\mathrm{d}x} = G_{op} - R(x) \tag{2}$$

$$\frac{1}{q}\frac{\dot{\mathrm{d}}J_n}{\mathrm{d}x} = -G_{op} + R(x) \tag{3}$$

J_P is hole current density, J_n is electron current density, G_{op} is carrier generation rate, and and R is the total recombination rate.

$$J_n = qn\,\mu_{\,n}E + \,qD_n\frac{\dot{\mathrm{d}}n}{\mathrm{d}x} \tag{4}$$

$$J_p = qn\,\mu_{\,p}E + \,qD_p\frac{\dot{\mathrm{d}}p}{\mathrm{d}x} \tag{5}$$

where D_p and D_n are diffusion coefficients of hole and electron, respectively, E is the electric field, and μ_P and μ_n are hole and electron mobilities, respectively.

Fig. 1 shows a schematic diagram of a $MAPbI_3$ perovskite solar cell, which is composed of three main layers: ZrS_2 as electron transport material (ETL), $MAPbI_3$ as absorber materials, and GO layer as hole transport layer (HTL) fabricated between two electrodes; the back contact metal electrode is gold (Au), and the front contact electrode is fluorine-doped tin oxide (SnO_2:F).

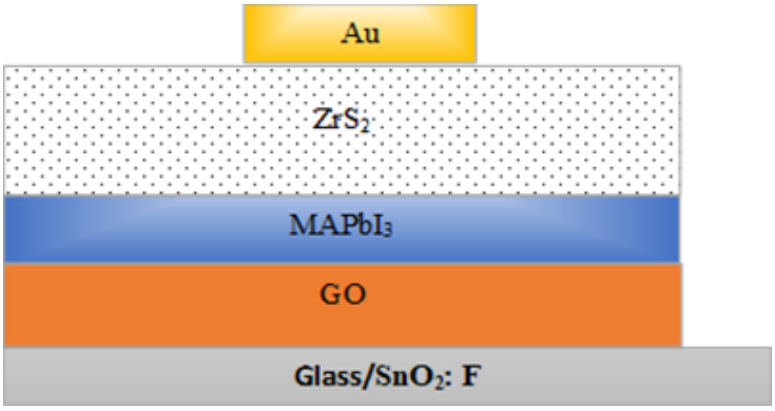

Fig. 1 – Schematic diagram of Au/ZrS_2/$MAPbI_3$/GO /SnO_2:F solar cell.

To operate accurate and precise simulations, the SCAPS-1D tool necessitates the input of true physical parameters pertaining to the various material layers within the fabricated device (as depicted in Fig. 1). These parameters are summarized and detailed based on the literature in Table 1. Furthermore, SCAPS-1D offers the option to include information regarding the electrical properties of both the front and back contact electrodes, as outlined in Table 2 [10, 11, 22, 24].

Table 1

Simulation parameters of each layer of the proposed solar cell

Material property	ZrS_2	$MAPbI_3$	GO
Thickness (um)	1	0.4	0.2
Bandgap (ev)	1.2–1.7	1.55	3.25
Electron affinity (ev)	4.7	3.95	1.9
Dielectric permittivity (relative)	16.4	6.5	3
CB effective density of states ($1/cm^3$)	$2.2\ E^{+19}$	$3.97\ E^{+18}$	$2.2\ E^{+21}$
VB effective density of states ($1/cm^3$)	$1.8\ E^{+19}$	$3.97\ E^{+18}$	$1.8\ E^{+21}$
Electron mobility (cm^3/Vs)	300	2	100
Hole mobility (cm^3/Vs)	30	2	300
Shallow uniform donor density ND ($1/cm^3$)	$1.00\ E^{+19}$	$10.0\ E^{+13}$	0
Shallow uniform acceptor density NA ($1/cm^3$)	0	0	$1.00\ E^{+16}$

Table 2

Simulation parameters of back and front contacts of the proposed device

Parameter	Back contact (Au electrode)	Front contact (SnO_2:F electrode)
Surface recombination velocity of electrons (cm/s)	$1.00\ E^{+5}$	$1.00\ E^{+5}$
Surface recombination velocity of holes (cm/s)	$1.00\ E^{+7}$	$1.00\ E^{+7}$
Metal work function (ev)	5.1	4.4

3. RESULTS AND DISCUSSION

3.1. Effect of MAPI3 layer on the performance of GO/ZrS2 solar cells

Using SCAPS-1D simulation, the current density-voltage (J-V) characteristics of the Au/GO/$MAPbI_3$/ZrS_2/SnO_2:F and Au/GO/ZrS_2/SnO_2:F solar cells were studied starting at 0.0 V and incrementing in steps of 0.05 V up to +1.0 V. Fig. 2a shows the J-V characteristics of the Au/GO/$MAPbI_3$/ZrS_2/SnO_2:F solar cell on a linear scale. This solar cell produced an open circuit voltage (V_{oc}) of 0.9 V, short circuit current (J_{sc}) of 38.3 mA/cm^2, and power conversion efficiency, η, of 26.3%.

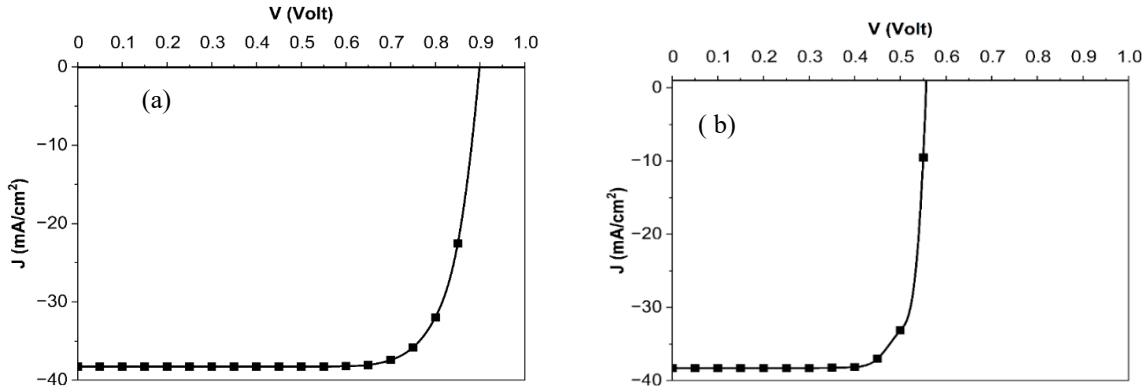

Fig. 2 – J-V characteristics of: (a) Au/GO/$MAPbI_3$/ZrS_2/SnO_2:F and (b) Au/GO/ZrS_2/SnO_2:F solar cells under illumination.

Conversely, as appears in Fig. 2b, the Au/GO/ZrS_2/SnO_2:F solar cell exhibited lower efficiency in comparison to the $MAPbI_3$ layer solar cell under illumination. It produced a V_{oc} of 0.55V, J_{sc} of 37 mA/cm^2, and a power conversion efficiency of 17% (Fig. 2b).

The performance differences between the two devices are due to the provision of a better junction generated from the mediated $MAPbI_3$ layer between the ZrS_2 and GO layers. Introducing this new layer ($MAPbI_3$) leads to a boost in efficiency and open circuit voltage (V_{oc}) from 17% to 26% and 0.55 V to 0.9 V, respectively. We attribute the observed enhancements to the energy gap difference between the used materials, which could affect the junction properties formed between $MAPbI_3$ and ZrS_2. According to Table 3, the HOMO and LUMO of the $MAPI_3$ layer are intermediate energy levels of ZrS_2 and GO, which serve as an absorber layer of light falling on the solar cells to generate hole and electron charges. The hole moves easily through the GO layer while the electron transports through the ZrS_2.

Table 3

Energy levels of $MAPI_3$, ZrS_2 and GO

Material	Bandgap (eV)	HOMO (eV)	LUMO (eV)	Reference
$MAPI_3$	1.5	–5,4	–3.9	[31]
ZrS_2	1.2–1.7	–6.1	–4.5	[24]
GO	1.5–3.2	–7.2	–4.0	[32]

The additional energy levels of the $MAPbI_3$ layer suppress the energy losses by controlling charge recombination and minimizing non-radiative pathways, which are responsible for voltage loss. This increases the potential barrier at the junction, thereby increasing the V_{oc}. Similar results were reported by Qingzhi An *et al*., whom observed a significant enhancement of the open circuit voltage (V_{oc}) of the device by introducing π-extended phosphonium fluorene electrolytes (π-PFEs) between phenyl-C61-butyric acid methyl ester (PCBM) and silver (Ag) in an $MAPbI_3$ solar cell [33]. In our previous report, the encapsulation of dye between P3HT and nc-TiO_2 in P3HT/dye/nc-TiO_2 led to an improvement in the solar cells' maximum electric power to 0.14 mW/cm^2, compared to 0.04 mW/cm^2 in the case the non-encapsulated solar cells [16]. In this context, it is worth mentioning that our presented solar cell system exhibits a better performance than other reported ZrS_2-based structures of perovskite solar cells. In 2023, Abdelfatah reported an efficiency of 23% for ZrS_2/CuO heterojunction solar cells, which was lower than that of Au/GO/$MAPbI_3$/ZrS_2/SnO_2:F solar cells by a margin of 3% [24].

Electrical capacity is an important dynamic parameter of photovoltaic (PV) systems and should be investigated because it can provide information about the health status and quality of PV modules. Figure 3 shows the capacitance curves over a wide range of frequencies for our Au/GO/$MAPbI_3$/ZrS_2/SnO_2:F tested solar cell system at different voltages. We observed that applying 1.0 V bias (Fig. 3a) boosts the capacitance by nearly two orders of magnitude as the frequency increases from 1.0 MHz to 10.0 KHz, indicating strong dispersion in the capacitive behavior. Conversely, this effect decreases to approximately one order of magnitude when the bias voltage is reduced to 0.5 V (Fig. 3b), covering frequencies from 10 MHz to 100 KHz. Additionally, an enhancement in the capacitance was observed when the applied voltage increased from 0.0 to 1.0 V, as explained by the transient response of the solar cell's capacitance during changes in voltage in Fig. 3.

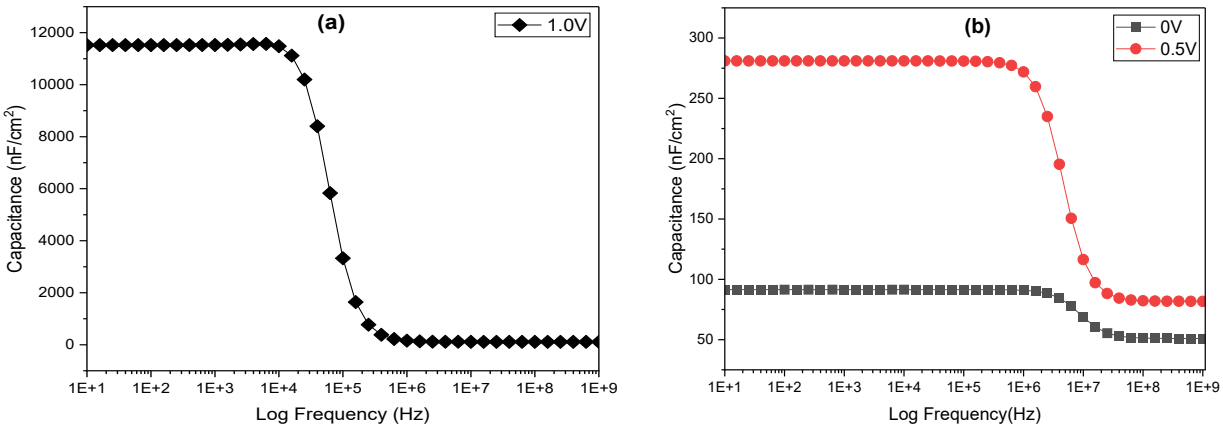

Fig. 3 – Characteristics of Au/GO/$MAPbI_3$/ZrS_2/SnO_2:F solar cells under: (a) 1.0 V and (b) 0.0 and 0.5 V bias conditions.

In the case of the Au/GO/ZrS_2/SnO_2:F solar cell system, the capacitance curves over a wide range of frequencies at different applied voltages are shown in Figs. 4a and 4b.

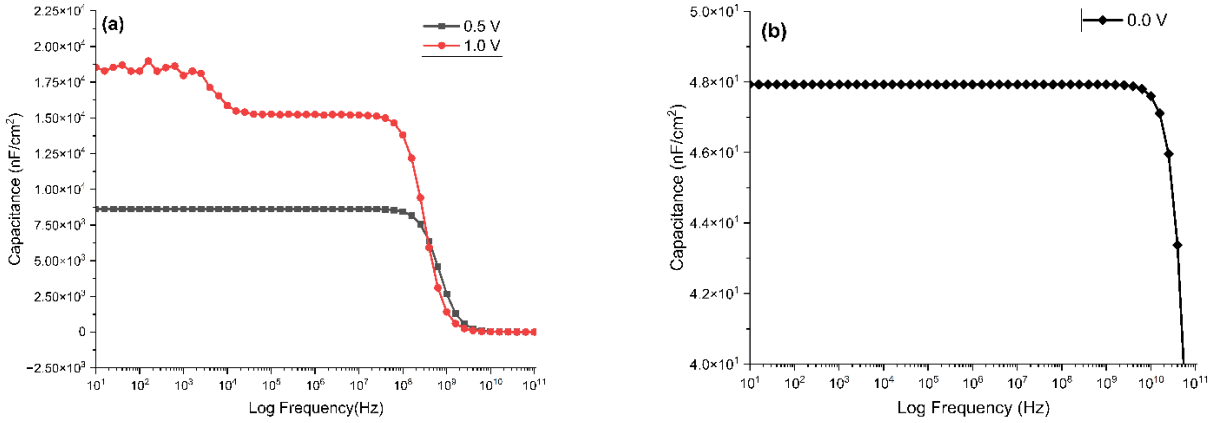

Fig. 4 – Characteristics of SnO_2:Fn/ZrS_2/GO/AU solar cells at: (a) 0.5 and 1.0 V, and (b) 0.0 V voltage bias condition.

At a constant bias voltage of 1 V, a significant decrease in capacitance was observed with decreasing frequency in the range of 100 MHz to 1 GHz. Compared to the Au/GO/$MAPbI_3$/ZrS_2/SnO_2:F solar cell system. The capacitance decreased by approximately 3 orders of magnitude. Similarly, a two-fold decrease in capacitance was observed from 100 MHz to 10 GHz when a bias voltage of 0.5 V was applied (Fig. 4a). Additionally, the dispersion in the capacitive behavior of two-layer solar cells was observed at higher frequencies than in the three-layer system.

The capacitance-frequency (C-F) results of SnO_2:Fn/ZrS_2/GO/AU and SnO_2:Fn/ZrS_2/$MAPbI_3$/GO/AU solar cells may be interpreted by defining an equivalent circuit (EC) of the two solar cells. Fig. 5 shows the AC model composed of three RC parts. The symbols in Fig. 5 are as follows:

- C_{b1} and C_{b2} represent the capacitance of the bulk region of GO and ZrS_2, respectively. C_j represents the capacitance of the interface between GO and ZrS_2.
- R_{b1} and R_{b2} represent the resistance of the bulk region of GO and ZrS_2, respectively. R_j represents the resistance of the interface between GO and ZrS_2.

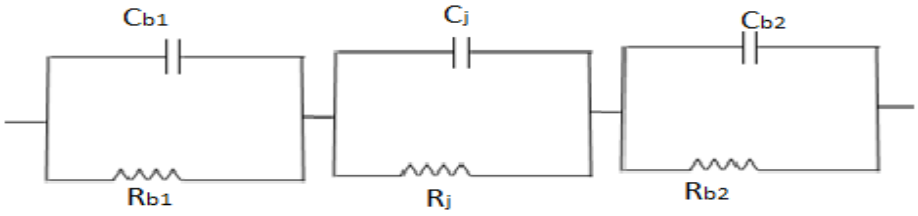

Fig. 5 –Equivalent circuits of GO/$MAPbI_3$/ZrS_2 and GO/ZrS_2 solar cells.

As shown in Figs. 3 and 4, the high-frequency capacitance of GO/$MAPbI_3$/ZrS_2 and GO/ZrS_2 remains constant as voltage is applied to the device. This capacitance is dominated by the smallest of the series capacitances, *i.e.*, the bulk capacitances in the circuit of Fig. 5. The total capacitance (C_{total}) is expressed by

$$\frac{1}{c_{\text{total}}} = \frac{1}{c_{b1}} + \frac{1}{c_{b2}} + \frac{1}{c_j} \tag{6}$$

C_j is the capacitance of the junction and arises from the depletion region capacitance and diffusion capacitance, *i.e.*,

$$c_j = c_{deple} + c_{diff} \tag{7}$$

The high-frequency capacitance of the two solar cells exhibits mostly minimal variation over a range of 100 GHz to 0.1 GHz, dominated by the geometric capacitance (C_G) of solar cells. Meanwhile, the junction

capacitance may not contribute to the total capacitance under these conditions [16, 20]. This latter feature can be attributed to the fact that charge carriers at the junction do not respond quickly to the change in AC signal, whereas C_G mainly depends only on the thickness and dielectric materials of the composition of solar cells. Thus, there is a reduction in the material's ability to store electric charge effectively and a decrease in the material's capacitance at high frequencies. Under high forward bias conditions (1.0 V), the initial increase in capacitance of the two devices was at frequencies of 10^5 Hz and 10^9 Hz for GO/$MAPbI_3$/ZrS_2 and GO/ZrS_2 solar cells, respectively. This difference can be attributed to the distinct electronic properties and charge carrier dynamics of the materials involved, particularly within their interfaces. GO/$MAPbI_3$/ZrS_2 solar cells may exhibit capacitance changes at lower frequencies due to longer carrier lifetimes within the perovskite layer. Conversely, GO/ZrS_2 solar cells may demonstrate faster carrier dynamics leading to capacitance changes at higher frequencies. In fact, it is well known that the charge carrier lifetime is a crucial parameter in solar cells [34]. Hence, if the charge carriers need more time to reach the collection electrodes before recombining with each other or defects in the material, the efficiency of the solar cells is minimized. In GO/$MAPbI_3$/ZrS_2 solar cells, there are multiple junctions: one between GO/$MAPbI_3$ and one between $MPbI_3$/ZrS_2 with varying material band-gaps. These differences reduce the chances of carriers recombining before contributing to the photocurrent and capturing a broader spectrum of photons. Thus, there are fewer losses of charge carriers, resulting in higher open circuit voltage. As we presented previously, the suggested GO/$MAPbI_3$/ZrS_2 solar cell system exhibited a 0.9 V open circuit voltage and 26% efficiency. Contrarily, in GO/ZrS_2 solar cells, without the additional junctions and band-gap variation provided by the $MAPbI_3$ layer, the efficiency may be lower due to less effective light absorption and increasing charge carrier recombination besides their faster carrier dynamics [35]. This is accompanied by a low open circuit voltage of 0.5 V and efficiency of 17%. This agrees with the results of Ding, which suggested dominant charge carrier recombination at the interface and worsened open-circuit voltage (V_{oc}) if the conduction band minimum of the electron transport material (ESL) is lower than that of the perovskite [36].

Moreover, as shown in Figs. 3 and 4, the frequency dependence of capacitance shows a significant decrease in the range from 10^{10} Hz to 10^8 Hz. This behavior indicates junction capacitance, the dominant mechanism of GO/ZrS_2 solar cells at these frequencies. The depletion region capacitance mainly contributes to the junction capacitance, and the influence of the diffusion capacitance is minimal (see Equation 7). This can be explained by decreasing the barrier potential or width of the depletion region between the GO and ZrS_2 and the weakness of the electric field that separates the charge carriers. Consequently, there is a high probability that the photo charge carriers (electron-hole pair) may recombine before reaching the electrodes, producing low open circuit voltage. For the GO/$MAPbI_3$/ZrS_2 solar cell, the measured capacitance increased when the frequency decreased from 10^5 Hz to 10^3 Hz and is dominated by the junction capacitance. This capacitance is higher than the capacitance of the GO/ZrS_2 solar because the diffusion capacitance dominates it, unlike in GO/ZrS_2 solar cells. We attributed this observation to the presence of the $MAPbI_3$ layer, which minimizes the effect of the depletion region. The $MAPbI_3$ layer has a relatively high charge carrier mobility; thus, the charge carriers can diffuse relatively quickly through this material. Based on our results, increasing the open circuit voltage to 0.9 V is proof of the reduction of charge carrier recombination. To emphasize the difference in properties of the two devices, the C-V characteristics of solar cells with and without the $MAPbI_3$ layer were measured as a function of applied bias voltage at 10 kHz. The resulting capacitance-voltage plots are shown in Fig. 6.

In ZrS2/$MAPbI_3$/GO solar cells, the capacitance exhibits negligible dependence on the applied voltage under reverse bias conditions (from −1 V to 0 V). However, a significant increase in capacitance is observed at 0.5 V forward bias. This voltage is called the onset voltage and represents a significant change in the internal energy status of the device. Similarly, in ZrS_2/GO solar cells, the capacitance also remains constant during reverse bias but shows a rapid increase in capacitance at the onset voltage of 0.25 V. Additionally, the capacitance of the two devices passes through a maximum and decreases rapidly with a further increase towards the forward bias, especially in ZrS_2/$MAPbI_3$/GO solar cells. We believe that the latter differences are further evidence of how the presence of $MAPbI_3$ layers changes the properties of the interface, through producing high onset voltage. The high onset voltage of capacitance indicates a higher built-in voltage or barrier potential within the solar cell, which contributes to a higher open-circuit voltage [37]. Therefore, ZrS_2/GO solar cells produce an open circuit voltage, V_{oc}, of 0.5 V, while ZrS_2/$MAPbI_3$/GO solar cells produce a V_{oc} of 0.92 V.

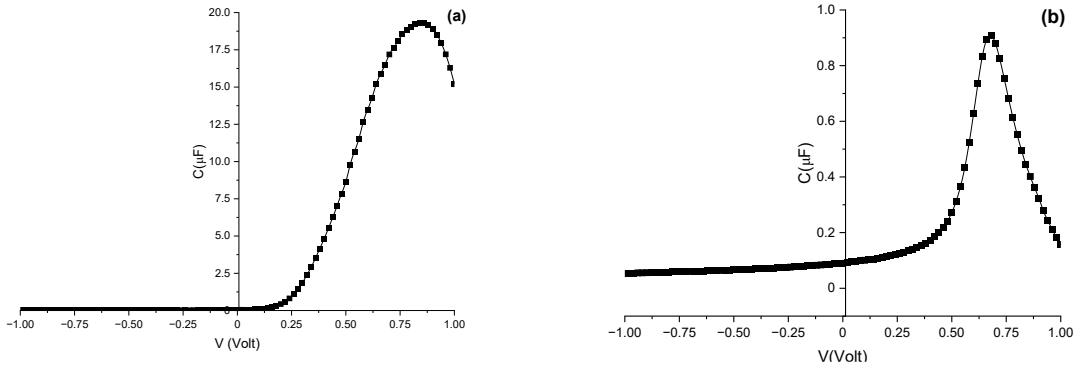

Fig. 6 – The C-V characteristics of: (a) ZrS_2/ $MAPbI_3$/GO and (b) ZrS_2/ GO solar cells at +10KHZ.

4. CONCLUSIONS

The results in the present work show the impact of incorporating $MAPbI_3$ interlayer on the performance of ZrS_2/GO hetero-junction solar cells using SCAPS-1D simulation. The emergence of the $MAPbI_3$ layer between the ZrS_2 and GO layers in the solar cell has led to significant improvements in key photovoltaic parameters. The V_{oc} and η improved from 0.55 to 0.9 V and from 17 to 26%, respectively. In the GO/$MAPbI_3$/ZrS_2 solar cells system, these enhancements can be attributed to the formation of multiple junctions and variations in band gaps between the layers. These variations can enhance light absorption and prolong the lifetime of charge carriers, which are crucial to enhancing the η of solar cells. The C-F and C-V analyses validate these observations. GO/$MAPbI_3$/ZrS_2 solar cell exhibited a larger onset voltage of capacitance, representing a larger build-in potential and reduced recombination of charge carriers at interfaces. While, GO/ZrS_2 solar cell exhibited reduced capacitance and increased carrier dynamics, responsible for reduced efficiency and V_{oc}. Insertion of the $MAPbI_3$ layer effectively lessens the depletion region impact, and charge carriers can diffuse and collect effectively, aided through increased capacitance behavior. The results confirm the critical role played by interfacial engineering in perovskite solar cells. This work paves a window for future studies in terms of offering useful information for future perovskite solar cells' development, with a strong emphasis placed on selecting materials and configuration of layers for overcoming efficiency barriers. Experimental verification of these observations and device engineering for even improved performance values can be taken in future work.

ACKNOWLEDGEMENTS

The authors would like to acknowledge the support of the Deanship of Scientific Research of Mutah University through research project #339/2020. The authors are also thankful to Prof. Marc Burgelman, University of Gent, Belgium, for providing the SCAPS-1D software for our study.

REFERENCES

[1] Holechek JL, Geli HME, Sawalhah MN, Valdez R. A global assessment: Can renewable energy replace fossil fuels by 2050? Sustainability. 2022; 14: 4792. DOI: 10.3390/su14084792.

[2] Perera F. Pollution from fossil-fuel combustion is the leading environmental threat to global pediatric health and equity: Solutions exist. Int J Environ Res Public Health. 2017; 15: 16. DOI: 10.3390/ijerph15010016.

[3] Jiries A, Al-Nasir F, Hijazin TJ, Al-Alawi M, El Fels L, Mayyas A, *et al*. Polycyclic aromatic hydrocarbons in citrus fruit irrigated with fresh water under arid conditions: Concentrations, sources, and risk assessment. Arab J Chem. 2022; 15(9): 104027. DOI: 10.1016/j.arabjc.2022.104027.

[4] Al-Nasir F, Hijazin TJ, Al-Alawi MM, Jiries A, Mayyas A, S AA-D, *et al*. Accumulation, source identification, and cancer risk assessment of polycyclic aromatic hydrocarbons (PAHs) in different jordanian vegetables. Toxics. 2022; 10: 643. DOI: 10.3390/toxics10110643.

[5] Al-Madanat O, AlSalka Y, Ramadan W, Bahnemann DW. TiO_2 photocatalysis for the transformation of aromatic water pollutants into fuels. Catalysts. 2021; 11: 317. DOI: 10.3390/catal11030317.

[6] Ombaka LM, McGettrick JD, Oseghe EO, Al-Madanat O, Rieck Genannt Best F, Msagati TAM, *et al*. Photocatalytic H_2 production and degradation of aqueous 2-chlorophenol over B/N-graphene-coated Cu^0/TiO_2: A DFT, experimental and mechanistic investigation. J Environ Manage. 2022; 311: 114822. DOI: 10.1016/j.jenvman.2022.114822.

[7] Maka AOM, Alabid JM. Solar energy technology and its roles in sustainable development. Clean Energy. 2022; 6: 476–483. DOI: 10.1093/ce/zkac023.

[8] Al-Dmour H, Al-Trawneh S, Al-Taweel S. Synthesis, characterization, and performance of oligothiophene cyanoacrylic acid derivatives for solar cell applications. IJAAS. 2021; 8: 128–135. DOI: 10.21833/ijaas.2021.06.015.
[9] Al-Dmour H, Taylor DM. Small-signal response of nanocrystalline-titanium dioxide/poly(3-hexylthiophene) heterojunction solar cells. Thin Solid Films. 2011; 519: 8135–8138. DOI: 10.1016/j.tsf.2011.06.009.
[10] Al Dmour H. SCAPS numerical analysis of graphene oxide /TiO_2 bulk heterojunction solar cell sensitized by N719 Ruthenium dye. East Eur J Phys. 2023: 555–561. DOI: 10.26565/2312-4334-2023-3-65.
[11] Mousa MS, Al Dmour H, Jaradat EK, Al-Madanat OY, Jaber AMD, Zaidi B, *et al*. Studying the effect of transport layers on ZrS2/MEH-PPV solar cells: using SCAPS-1D software. East European Journal of Physics 2024: 419–426. DOI: 10.26565/2312-4334-2024-4-49.
[12] Ramanujam J, Singh UP. Copper indium gallium selenide based solar cells – a review. Energy Environ Sci. 2017; 10: 1306–1319. DOI: 10.1039/c7ee00826k.
[13] Khatibi A, Razi Astaraei F, Ahmadi MH. Generation and combination of the solar cells: A current model review. Energy Sci Eng 2019; 7: 305–322. DOI: 10.1002/ese3.292.
[14] Shah N, Shah AA, Leung PK, Khan S, Sun K, Zhu X, *et al*. A review of third generation solar cells. Processes. 2023; 11: 1852. DOI: 10.3390/pr11061852.
[15] Kafashan H, Bahrami A. CIGS solar cells using ZrS_2 as buffer layer: Numerical simulation. Optik. 2024; 298: 171594. DOI: 10.1016/j.ijleo.2023.171594.
[16] Al-Dmour H, Alzard RH, Alblooshi H, Alhosani K, AlMadhoob S, Saleh N. Enhanced energy conversion of Z907-based solar cells by Cucurbit[7]uril Macrocycles. Front Chem. 2019; 7: 561. DOI: 10.3389/fchem.2019.00561.
[17] Saleh N, Al-Trawneh S, Al-Dmour H, Al-Taweel S, Graham JP. Effect of molecular-level insulation on the performance of a dye-sensitized solar cell: fluorescence studies in solid state. J Fluoresc. 2015; 25: 59–68. DOI: 10.1007/s10895-014-1479-8.
[18] Boix PP, Nonomura K, Mathews N, Mhaisalkar SG. Current progress and future perspectives for organic/inorganic perovskite solar cells. Mater Today. 2014; 17: 16–23. DOI: 10.1016/j.mattod.2013.12.002.
[19] Kojima A, Teshima K, Shirai Y, Miyasaka T. Organometal halide perovskites as visible-light sensitizers for photovoltaic cells. J Am Chem Soc. 2009; 131: 6050–6051. DOI: 10.1021/ja809598r.
[20] Farooq WA, Atif M, Fatehmulla A, Yahia IS, AlSalhi MS, Fakhar-e-Alam M, *et al*. Photovoltaic and capacitance measurements of solar cells comprise of Al-doped CdS (QD) and hierarchical flower-like TiO_2 nanostructured electrode. Results Phys. 2020; 16: 102827. DOI: 10.1016/j.rinp.2019.102827.
[21] Best Research-Cell Efficiency Chart 2025. https://www.nrel.gov/pv/cell-efficiency.html [updated 2025].
[22] Raoui Y, Ez-Zahraouy H, Tahiri N, El Bounagui O, Ahmad S, Kazim S. Performance analysis of $MAPbI_3$ based perovskite solar cells employing diverse charge selective contacts: Simulation study. Sol Energy. 2019; 193: 948–955. DOI: 10.1016/j.solener.2019.10.009.
[23] Nazeeruddin MK, Snaith H. Methylammonium lead triiodide perovskite solar cells: A new paradigm in photovoltaics. MRS Bulletin. 2015; 40: 641–645. DOI: 10.1557/mrs.2015.169.
[24] Abdelfatah M, El Sayed AM, Ismail W, Ulrich S, Sittinger V, El-Shaer A. SCAPS simulation of novel inorganic ZrS_2/CuO heterojunction solar cells. Sci Rep. 2023; 13: 4553. DOI: 10.1038/s41598-023-31553-4.
[25] Jeong WL, Park SH, Jho YD, Joo SK, Lee DS. The role of the graphene oxide (GO) and reduced graphene oxide (RGO) intermediate layer in CZTSSe thin-film solar cells. Materials. 2022; 15: 3419. DOI: 10.3390/ma15103419.
[26] Han Y, Meyer S, Dkhissi Y, Weber K, Pringle JM, Bach U, *et al*. Degradation observations of encapsulated planar $CH_3NH_3PbI_3$ perovskite solar cells at high temperatures and humidity. J Mater Chem. 2015; 3: 8139–8147. DOI: 10.1039/c5ta00358j.
[27] Ava TT, Al Mamun A, Marsillac S, Namkoong G. A review: Thermal stability of methylammonium lead halide based perovskite solar cells. Appl Sci. 2019; 9: 188. DOI: 10.3390/app9010188.
[28] Burgelman M, Nollet P, Degrave S. Modelling polycrystalline semiconductor solar cells. Thin Solid Films. 2000; 361–362: 527–532. DOI: 10.1016/s0040-6090(99)00825-1.
[29] Zerfaoui H, Dib D, Rahmani M, Benyelloul K, Mebarkia C. Study by simulation of the SnO_2 and ZnO anti-reflection layers in n-SiC/p-SiC solar cells. AIP Conf Proc. 2016; 1758: 030029. DOI: 10.1063/1.4959425.
[30] Mehmood S, Xia Y, Qu F, He M. Investigating the performance of efficient and stable planer perovskite solar cell with an effective inorganic carrier transport layer using SCAPS-1D simulation. Energies. 2023; 16: 7438. DOI: 10.3390/en16217438.
[31] Chang T-W, Tseng C-C, Chen DW, Wu G, Yang C-L, Chen L-C. Preparation and characterization of thin-film solar cells with Ag/C60/$MAPbI_3$/CZTSe/Mo/FTO multilayered structures. Molecules. 2021; 26: 3516.
[32] Carminati SA, Rodríguez-Gutiérrez I, de Morais A, da Silva BL, Melo MA, Souza FL, *et al*. Challenges and prospects about the graphene role in the design of photoelectrodes for sunlight-driven water splitting. RSC Adv. 2021; 11: 14374–14398. DOI: 10.1039/D0RA10176A.
[33] An Q, Sun Q, Weu A, Becker-Koch D, Paulus F, Arndt S, *et al*. Enhancing the open-circuit voltage of perovskite solar cells by up to 120 mV using π-Extended phosphoniumfluorene electrolytes as hole blocking layers. Adv Energy Mater. 2019; 9: 1901257. DOI: 10.1002/aenm.201901257.
[34] Kiermasch D, Rieder P, Tvingstedt K, Baumann A, Dyakonov V. Improved charge carrier lifetime in planar perovskite solar cells by bromine doping. Sci Rep. 2016; 6: 39333. DOI: 10.1038/srep39333.
[35] Chen T, Chen WL, Foley BJ, Lee J, Ruff JPC, Ko JYP, *et al*. Origin of long lifetime of band-edge charge carriers in organic-inorganic lead iodide perovskites. Proc Natl Acad Sci. 2017; 114: 7519–7524. DOI: 10.1073/pnas.1704421114.
[36] Ding C, Zhang Y, Liu F, Kitabatake Y, Hayase S, Toyoda T, *et al*. Effect of the conduction band offset on interfacial recombination behavior of the planar perovskite solar cells. Nano Energy. 2018; 53: 17–26. DOI: 10.1016/j.nanoen.2018.08.031.
[37] Kirchartz T. High open-circuit voltages in lead-halide perovskite solar cells: experiment, theory and open questions. Philos Trans A Math Phys Eng Sci. 2019; 377: 20180286. DOI: 10.1098/rsta.2018.0286.

Received January 1, 2025